

ASCA Observation of an “X-ray Shadow” in the Galactic Plane

Sangwook Park and Ken Ebisawa

*Laboratory for High Energy Astrophysics, Code 662
NASA/Goddard Space Flight Center, Greenbelt, MD. 20771*

and

Universities Space Research Association

spark@lobster.gsfc.nasa.gov, ebisawa@olegacy.gsfc.nasa.gov

ABSTRACT

The diffuse X-ray background (DXB) emission near the Galactic plane ($l, b \sim 25.6^\circ, 0.78^\circ$) has been observed with *ASCA*. The observed region is toward a Galactic molecular cloud which was recently reported to cast a deep X-ray shadow in the 0.5 – 2.0 keV band DXB. The selection of this particular region is intended to provide a constraint on the spatial distribution of the DXB emission along the line of sight: i.e., the molecular cloud is optically thick at <2 keV and so the bulk of the observed soft X-rays *must* originate in the foreground of the cloud, which is at ~ 3 kpc from the Sun. In the 0.8 – 9.0 keV band, the observed spectrum is primarily from multiple components of thermal plasmas. We here report a detection of soft X-ray (0.5 – 2 keV) emission from an $\sim 10^7$ K thermal plasma. Comparisons with the *ROSAT* data suggest that this soft X-ray emission is absorbed by $N_H = 1 - 3 \times 10^{21}$ cm $^{-2}$, which implies a path-length through the soft X-ray emitting regions of $\lesssim 1$ kpc from the Sun.

Subject headings: diffuse radiation — Galaxy: structure — ISM: structure — X-rays: ISM

1. INTRODUCTION

The 0.1 – 0.3 keV band diffuse X-ray background (DXB) emission in the Galactic plane has been attributed to the emission from the Local Hot Bubble (LHB): an $\sim 10^6$ K plasma filling an extensive cavity, where absorbing neutral material is deficient, with an average radius of ~ 100 pc around the solar system (Cox & Reynolds 1987; Snowden et al. 1998). At >2 keV it has been known that there exists unresolved DXB emission along a thin disk of the plane ($-60^\circ < l < 60^\circ$): the so-called Galactic ridge X-ray emission (GRXE) (Worrall et al. 1982; Warwick et al. 1985).

The detection of the Fe K line emission, with a scale height of ~ 100 pc (Yamauchi & Koyama 1993), revealed the thermal origin of the GRXE (Koyama et al. 1986a). Unresolved point sources would be insufficient to produce the observed X-ray flux (Yamauchi et al. 1997; Yamasaki et al. 1997), and the bulk of the GRXE appears to have diffuse origins such as multiple supernova remnants (Koyama et al. 1986b; Kaneda et al. 1997; Valinia & Marshall 1998). The implied temperature for the thermal plasma to make up the 2 – 10 keV GRXE ranges $\sim 10^{7.5}$ – $\sim 10^8$ K (Koyama et al. 1986a; Kaneda et al. 1997; Yamauchi et al. 1997; Valinia & Marshall 1998).

The nature of the 0.5 – 2 keV band DXB along the plane is elusive. The presence of a few million K Galactic gas beyond the LHB and nearby supernova remnants has been suggested in order to incorporate the observed soft X-ray emission in the plane (Nousek et al. 1982). The distribution and the spectral properties of the X-ray emitting material along the line of sight have yet to be known. One of the major advances in the study of the 0.5 – 2 keV band Galactic DXB in the plane came with the detection of “X-ray shadows” cast by distant molecular clouds. The X-ray shadows in the DXB as detected with mosaics of the *ROSAT* PSPC pointed observations in the Galactic plane have recently revealed the existence of a highly enhanced X-ray emitting region (i.e., the derived X-ray background intensity beyond the absorbing molecular clouds is more than an order of magnitude brighter than the nominal high latitude intensity) around the Galactic center: the Galactic X-ray bulge (GXB) (Park et al. 1997; Almy et al. 2000; Park et al. 1998, P98 hereafter). The estimated plasma temperature of the GXB is $\sim 10^{6.6-6.7}$ K. These results are in good agreement with the *ROSAT* all-sky survey (RASS) data analysis in the general direction of the Galactic center (Snowden et al. 1997). P98 further suggested that the angular extension of the GXB along the first quadrant of the plane may be confined by the molecular ring at $l \sim 25^\circ$.

The results of these X-ray shadow studies also suggest that there exists a substantial fraction of DXB emission originating foreground to the absorbing molecular clouds, which are located at 2 – 3 kpc from the Sun. The “foreground component” was tentatively attributed to the emission from a $\sim 10^7$ K plasma based on a band-fraction analysis (Park 1998). The extensive spectral analyses of individual DXB components along the line of sight were however infeasible with the *ROSAT* PSPC data due to the limited spectral capabilities of the PSPC mosaics.

In order for a spectral study of the Galactic DXB originating foreground to the X-ray shadow clouds, we carried out an *ASCA* observation in the direction of $l, b = 25.6^\circ, 0.78^\circ$. The $l, b = 25.6^\circ, 0.78^\circ$ direction is toward a Galactic molecular cloud which was recently reported to cast an X-ray shadow in the 0.5 – 2.0 keV band (P98). The existence of the dense molecular cloud with a well-established kinematic distance ($d \sim 3$ kpc) is expected to provide a useful constraint for the spatial distribution of the DXB emission along the line of sight. In other words, in the soft energy band (< 2 keV), the molecular cloud is optically thick and the distance to the cloud (~ 3 kpc) sets a *limit* for the X-ray emitting region, or regions, along the line of sight. The contribution from unresolved stellar sources to the observed 0.5 – 2 keV band DXB in the plane has been shown to be small (Schmitt & Snowden 1990; Wang 1992; Ottmann & Schmitt 1992). *ASCA* observations of the Scutum arm region ($l \sim 28^\circ - 29^\circ$) have also demonstrated that only $\sim 1\%$ of the DXB

emission in the plane is from unresolved point sources (Yamauchi et al. 1997). The bulk of the DXB in the plane is therefore *truly* diffuse. We can thus perform the spectral study of the 0.5 – 2 keV Galactic DXB emission, the bulk of which is diffuse and originates within ~ 3 kpc from the Sun. Utilizing the full effective energy range of *ASCA*, the overall spectrum is analyzed and is compared with the previous studies of the GRXE which were performed at different directions in the sky. The observation is described in §2. The analysis and results are presented in §3 and the implications are discussed in §4. A summary and the conclusions are presented in §5.

2. OBSERVATION

The *ASCA* observation in the direction of $l, b = 25.6^\circ, 0.78^\circ$ was carried out on 1998 March 31 during the AO6 phase. The data from the Gas Imaging Spectrometer (GIS) were obtained in the pulse-height (PH) mode and the total exposure for each detector (GIS2 and GIS3) is ~ 38 ks. For the analysis the data are integrated over two detectors for the inner 30' diameter circular region. The pointing direction ($l, b = 25.6^\circ, 0.78^\circ$) is centered on a Galactic molecular cloud which has an angular extent of $\sim 1^\circ$ to cast a deep X-ray shadow in the 0.5 – 2.0 keV band (P98). The exposure and vignetting corrected GIS images are displayed in Figure 1. Figure 1a is the hard band (2.0 – 9.0 keV) image and Figure 1b is the soft band (0.8 – 2.0 keV) image of the inner 30' diameter region. The observed count rate is 0.18 ± 0.002 counts s^{-1} within 30' diameter in the 0.8 – 9.0 keV band. There is a faint point-like source detection within 30' diameter, at RA(J2000)= $18^h 34^m 52^s.3$, Dec(J2000)= $-06^\circ 16' 37''.1$, in the 0.8 – 9 keV band. The source counts within 3' radius detection circle is, however, small ($\sim 1\%$ of the total counts).

The Solid-state Imaging Spectrometer (SIS) imposes some problems for the study of faint diffuse background emission. The SIS has experienced a decrease in detector efficiency and an increasing divergence from the GIS spectra since the early phase of the mission due to the accumulated radiation damage and the increasing fluctuation of the dark current. This degradation of the SIS performance can be substantial for the faint X-ray background spectra since the position dependence of the SIS performance change is not known for the *diffuse* background emission. The SIS also has a smaller effective area which also makes it inappropriate for the study of the faint diffuse background emission. The count rate for the SIS is ~ 0.07 counts s^{-1} even with the full effective solid angle (~ 480 arcmin²), which is only $\sim 39\%$ of the GIS count rate of the inner 30' diameter region. Considering that the photons detected near the edge of the nominal field of view may not be useful for the analysis, the number of utilizable photons with the SIS would be smaller than that of the GIS (30' diameter) at least by a factor of 4 – 5. In this paper we thus present only the GIS result which is free from systematic uncertainties and more reliable than SIS.

3. ANALYSIS & RESULTS

3.1. X-ray Images

The observed X-ray emission is smooth with no significant contribution from point sources (Figure 1). In order to investigate the distribution of the X-ray intensity over the field of view, radial profiles of the observed count rates for the non-cosmic X-ray background (NXB), data, and the cosmic X-ray background (CXB) components are compared. The NXB counts can be extracted with the night-Earth data. The night-Earth data are available from the HEASARC *ASCA* Guest Observer Facility (GOF), which is an accumulation of the data from 1993 June to 1999 August. Since the night-Earth background is known to have long-term variations over the years, the data taken only between 1998 January and 1998 May are extracted in order to accommodate the observation dates of our data. The CXB can be obtained with the “blank-sky” data released by the *ASCA* GOF at HEASARC, which are point-source removed high latitude observations taken between 1993 June and 1995 December. Since the CXB is presumably isotropic over the entire sky with no intensity variations, the blank-sky data can be utilized to test the angular distribution of our data. The observed data, night-Earth and blank-sky data are extracted in the soft (0.8 – 2 keV), the hard (2 – 9 keV), and the total (0.8 – 9 keV) band and the count rates are integrated over the annular bins of $1.5'$ within the $15'$ radius circular region.

The radial profiles of the 0.8 – 9 keV band average count rates in each bin are displayed in Figure 2. In Figure 2, the open-squares are observed data, filled-circles are the night-Earth count rates, open-circles are (data – night-Earth), and filled-squares are blank-sky. Although the night-Earth background generally has higher intensity around the edge of the detector (Ishisaki 1996), the effect is negligible within $15'$ from the center (Figure 2). Assuming the CXB intensity distribution is uniform over the sky, the intensity distribution of the X-ray data can be investigated by calculating the intensity ratio between the observed data and the blank-sky data. In Figure 2, the histograms present the radial profiles (arbitrarily scaled) of the data to blank-sky intensity ratio where the night-Earth contribution is subtracted from both. Within $15'$ radius of the nominal field of view, no statistically significant intensity variation is observed. The same analysis has been performed in the soft and the hard band. The results from these subbands also indicate no significant intensity variations over the field.

Since the effect of the shadow is not explicitly seen in the images, off-cloud observations may be necessary to assure the utility of the X-ray shadow in constraining the distribution of the soft DXB emission along the line of sight. No such observations are currently available leaving it for follow-up observations. The solid angle of our data is however only $30'$ diameter and is *completely* within the angular extent of the shadow. No intensity variation in the soft band image is thus not surprising considering no significant column variations around the central region of the cloud (P98) and the limited field of view for the data covering only the central region of the shadow. The smooth distribution in the hard band image may also be reasonable since the cloud is most likely *transparent* on average in the 2 – 9 keV band ($\tau \ll 1$). There may be some contribution

from the off-cloud emission due to the “stray-light” effect (see §3.2). For example, the contribution from offset angle $> 1^\circ$ is expected to be $\lesssim 15\%$ of the total counts in the 1 – 2 keV band (the contribution in the hard band is expected to be smaller) (Ishisaki 1996). The bulk of the observed flux in the soft band is thus assumed to arise in on-cloud region presumably representing the X-ray emission originating in the foreground of the cloud.

3.2. Background subtraction & Energy response

The study of the diffuse background emission with *ASCA* is substantially affected by the *stray light*, which is a “leakage” of the photons from outside of the nominal field of view due to the broadly extended *ASCA* mirror responses (Serlemitsos et al. 1995). A specific energy response of the detector must be generated to resolve this problem. For this purpose an ancillary response file (ARF) for the diffuse emission is generated through ray-tracing, assuming an *uniform* X-ray emitter having 1.5° radius. This technique is essentially identical to those by Kaneda et al. (1997) and Valinia et al. (2000). Although the diffuse ARF is created for the Galactic diffuse emission, it is also used in determining the normalization for the extragalactic power law. This specific ARF is utilized in the following spectral analysis.

As the first step of the spectral analysis the NXB is subtracted using night-Earth data. The extragalactic power law component of the DXB (presumably from unresolved AGNs) then needs to be considered since the contribution from this component in the photon energy of >2 keV is significant even in the plane. The power law component of the DXB has been extensively studied with high latitude data and can be described with a photon index of $\Gamma \sim 1.4$ in the 2 – 10 keV band (Gendreau 1995; Chen et al. 1997). This extragalactic power law component is included in the spectral fitting as a fixed component. In order to produce an appropriate normalization of the power law component, blank-sky data are fitted with a simple power law model in the 0.8 – 9 keV band after subtracting the NXB. The best fit photon index is $\Gamma = 1.46$ ($\chi^2_\nu = 1.69$) which is consistent with previous results (Ishisaki 1996). A range of absorbing column density $N_H = 3 - 5 \times 10^{22} \text{ cm}^{-2}$ should be considered for the power law component accounting for the absorption by the Galactic plane assuming an average space density of 1 cm^{-3} in the Galactic disk. We found that the difference due to the assumed N_H values in this range does not affect the fit, and a fixed value of $N_H = 4 \times 10^{22} \text{ cm}^{-2}$ is used for the analysis.

3.3. Spectral Analysis

3.3.1. Raymond-Smith Model Fit

The observed spectrum should be associated with the GRXE, considering the observed dispersion and the effective energy band. For the study of the GRXE, optically thin thermal plas-

mas both in ionization equilibrium and non-equilibrium have been considered by previous authors (Koyama et al. 1986a; Yamasaki et al. 1997; Kaneda et al. 1997; Yamauchi & Koyama 1995; Valinia & Marshall 1998). With the *Ginga* data Yamauchi & Koyama (1995) have shown that the GRXE continuum temperature of 5 – 10 keV is too high for the detected 6.7 keV Fe line assuming an ionization equilibrium, and suggested a non-equilibrium state for the GRXE. A non-equilibrium ionization model was used by Kaneda et al. (1997) with *ASCA* data and the best fit temperature of ~ 7 keV was obtained for the hard component. On the other hand, presence of a power-law hard-tail in the GRXE spectrum in addition to the thermal components has been suggested (Yamasaki et al. 1997; Valinia & Marshall 1998). As a matter of fact, the GRXE as observed with *RXTE* was suggested to arise from an $\sim 2 - 3$ keV plasma in an ionization equilibrium as well as from a power law component of $\Gamma \sim 1.8$ which dominates at >10 keV (Valinia & Marshall 1998). The ionization state of the GRXE has thus been uncertain and the previous results have been dependent on different assumptions in the models.

Considering the complex nature of the modeling GRXE plasma, in this paper, we assume that thermal plasmas are in ionization equilibrium, as a first step toward the understanding of the nature of “X-ray shadow”. Our results in this paper may be subject to the assumption of ionization equilibrium, on which further investigations will be required. The spectral fitting is first performed with an absorbed Raymond-Smith (RS) model assuming thermal equilibrium. The best fit plasma temperature is $kT = 6.30^{+2.58}_{-1.25}$ keV with an absorption of $N_H = 0.55^{+0.13}_{-0.14} \times 10^{22} \text{ cm}^{-2}$ (the errors refer to a 90% confidence level, hereafter), where we used standard single absorption model (see §3.3.2). The best fit model is displayed in Figure 3. In Figure 3 the fixed extragalactic power law component is represented with a dashed line and the contribution is shown to be limited at $E > 2$ keV due to the absorption by the plane. It is clearly observed that the data are in good agreement with the model only at >2 keV (Figure 3), and the fit is unacceptable ($\chi^2_\nu = 3.63$) at <2 keV, the DXB in which energy band is motivation of the present work.

A second RS component is then added in the model. The fit is now good even at <2 keV ($\chi^2_\nu = 0.92$) and the overall statistics also improved ($\chi^2_\nu = 0.59$) (Figure 4). The soft component ($kT = 0.64^{+0.13}_{-0.16}$ keV with $N_H = 1.21^{+0.23}_{-0.29} \times 10^{22} \text{ cm}^{-2}$) makes up most ($\sim 75\%$) of the 0.5 – 2.0 keV band emission and the contribution from this component to the 2 – 10 keV band count rate is small ($\sim 6\%$). The hard component ($kT = 3.71^{+1.50}_{-0.79}$ keV) dominates the observed spectrum at >2 keV and produces $\sim 68\%$ of the count rates in the 2 – 10 keV band. The implied absorbing column of the hard component, $N_H = 2.47^{+1.13}_{-0.94} \times 10^{22} \text{ cm}^{-2}$, indicates that this component originates beyond the molecular cloud.

Even though the overall fit is good, the two component RS model imposes some discrepancies in the soft band. Since the molecular cloud is optically thick ($\tau \sim 1.7$ on average between 0.5 and 2 keV, P98) and so casts a deep X-ray shadow in the 0.5 – 2.0 keV band DXB, the bulk of the soft component *must* originate in the foreground of the cloud. The best fit absorbing column of the soft component ($N_H = 1.21 \times 10^{22} \text{ cm}^{-2}$), however, indicates a distance of $\gtrsim 3$ kpc through the emission region assuming an average space density of 1 cm^{-3} in the plane. This distance suggests

that the soft X-ray emitting region substantially extends beyond the cloud, which is inconsistent with the foreground origin for the soft component.

Furthermore, we found that this soft component does not agree with the *ROSAT* data on the same region. For a comparison with the *ROSAT* data, the best fit model is convolved with the *ROSAT* PSPC response and a hardness ratio is calculated. The 1.5 keV band (0.73 – 2.04 keV, corresponding to the R6 + R7 band for the *ROSAT* PSPC) to 0.75 keV band (0.44 – 1.21 keV, corresponding to the R4 + R5 band for the *ROSAT* PSPC) (Snowden et al. 1994) hardness ratio of the count rates for the modeled spectrum is 2.4. This hardness ratio is substantially higher than the observed value, 1.4, of the foreground count rates of the X-ray shadow in the same region as detected with *ROSAT* (P98).

3.3.2. Continuous Absorption Model

We have assumed a single “foreground” absorbing column for each RS component while, in reality, the X-ray emitting plasma and the absorbing material is more likely interspersed along the line of sight (Jakobsen & Kahn 1986). In order to investigate effects of the intermixture of the absorbing material and the X-ray emitting plasma, Kaneda (1996) has considered the “multi-absorption model” and found that the effect in the overall *ASCA* bandpass was not significant compared to the single foreground absorption. The “multi-absorption” model is still a more realistic picture especially in the soft band (< 2 keV) where the absorption is more sensitive to the distribution of the absorbing material along the line of sight.

In the following, we thus investigate both of the single and the “continuous” absorption model for the soft band emission. The single absorption is the case that the absorber is in front of the emitter, where we take the standard interstellar absorption model, such that $\exp(-N_H\sigma_H)$ is multiplied to the thermal plasma model. Here, N_H is the hydrogen column density, and σ_H is the average cross section per hydrogen atom by Morrison & McCammon (1983). We also consider the case that the emitter and absorber are completely intermingled and distributed uniformly along the line of sight. For this “continuous absorption model” we use the formula, $(1 - \exp(-N_H\sigma_H))/(N_H\sigma_H)$ instead. It is likely that the true distribution of the emitter and absorber will be somewhere in-between, so the model parameter ranges (such as N_H) we obtain using the two absorption models are considered to be conservative limits. For the hard component (> 2 keV), where the effect of the distribution of the absorbing material is not significant, only the single absorption utilizing the standard interstellar absorption is used in the following analysis.

3.3.3. Two Bremsstrahlung Models plus Gaussian Line Fits

The observed soft X-ray spectrum cannot be properly represented with the two component RS model, because the required soft component column density is too high and the hardness ra-

tio is inconsistent with the ROSAT result (§3.3.1). Note that the required column density would become even higher if we use the continuous absorption model (§4.1). Origin of the discrepancies may be in part due to our assumption of the full ionization equilibrium of the plasma. The soft band X-ray emitting plasma in the plane has been suggested to be in a non-equilibrium state (Kaneda et al. 1997) while we have assumed a thermal equilibrium. At least the RS model appears not effective to fit “unresolved” lines in the soft band spectrum as suggested by a systematic deviation in the residuals from the best fit model at $E < 2$ keV (Figure 4). As an attempt to improve the soft band spectral fitting, we fit the spectrum with two component thermal bremsstrahlung model with separate Gaussian components for the candidate atomic emission lines.

Kaneda et al. (1997) have detected several atomic line emission (e.g., Ne K, Fe L, Mg K, Si K, etc.) at < 2 keV in the Galactic plane DXB spectra, and our data show marginal evidence for emission lines at ~ 1.8 keV and ~ 1.3 keV in addition to the Fe line at ~ 6.7 keV (Figure 4). We thus fitted the observed spectrum with two component bremsstrahlung and three Gaussians. The best fit temperature for the continuum to make up the soft band emission is $kT \sim 10$ keV with low absorption and the hard band emission is from $kT \sim 2$ keV plasma being absorbed by $N_H \sim 3 \times 10^{22}$ cm $^{-2}$. Although the overall fit is good ($\chi^2_\nu = 0.48$), the best fit parameters appear unphysical by presenting a very high temperature plasma with a small absorption and a lower temperature plasma with a large absorption. This is unrealistic, since in the neighborhood of solar system, such a high temperature diffuse emission has not been detected. Also, this result contradicts with the more extensive observations of the GRXE by Kaneda et al. (1997), such that low temperature component is dominant in the lower energy band and so is the high temperature component in the higher energy band.

Although a simultaneous fitting with both soft and hard components is supposed to be ideal, such fitting is infeasible with low statistics of our data as we discussed above. We therefore decompose the observed spectrum in the hard and soft band to fit separately. Since the hard component shows a simpler spectral structure and has been more extensively studied by previous authors, we fit the hard component first and then fit the soft component with the hard component parameters fixed at the best fit values. For the hard component fitting a conservative cut-off at 3 keV, where the hard component dominates the observed GRXE spectrum (Kaneda et al. 1997), is taken for our data; i.e., in the 3 – 9 keV band, the spectrum is fitted with a thermal bremsstrahlung and a Gaussian line in order to determine the center energy of the Fe K line. The best fit line energy is $6.62^{+0.13}_{-0.14}$ keV where the continuum temperature is $kT = 3.67^{+4.16}_{-1.67}$ keV with an absorption of $N_H \sim 2.1 \times 10^{22}$ cm $^{-2}$ ($\chi^2_\nu = 0.45$). The temperature and the absorption values seem reasonable since previous observations indicate that the GRXE at 2 – 10 keV is from a $kT =$ a few keV plasma and that is distributed along a thin disk of the plane (Yamasaki et al. 1997; Koyama et al. 1986a; Kaneda et al. 1997). The line width was fixed at zero assuming a narrow emission line. When the line width is allowed to vary the best fit value is 233 eV with the uncertainty covering zero, which makes the narrow line assumption reasonable.

After determining the continuum temperature for the hard component and the Fe K line

energy, the line energies and continuum temperature for the soft band emission are fitted. Another bremsstrahlung model and two Gaussian components are added in the 0.8 – 9 keV band. The best fit line energies are $1.83_{-0.06}^{+0.07}$ keV and $1.23_{-0.08}^{+0.05}$ keV. The line widths are again set to zero assuming narrow lines as well as to help constrain fitted parameters. The best fit continuum temperature is $kT = 0.92_{-0.39}^{+0.41}$ keV. The associated absorption is negligible and a 2σ upper limit of 4.8×10^{21} cm^{-2} is obtained with the *continuous absorption* model. This implies a relatively nearby distance scale (probably <1.5 kpc, assuming a space density of 1 cm^{-3}) through the X-ray emitting regions, which is in good agreement with the assumption of the foreground (to the cloud) origin of the soft component. The overall fit is good with $\chi^2_{\nu} = 0.45$. The best fit model is displayed in Figure 5 and the model parameters are presented in Table 1. In Table 1 the results from the same model fitting with the *single absorption* for the soft component are also presented. The difference in the best fit parameters between the two models are insignificant. The 1.83 keV line can be identified with the Si K line. The identification of the “1.23 keV line” is unclear and may represent a blend of unresolved lines such as Mg K (1.35 keV) and Fe L (1.08 keV) lines as detected by Kaneda et al. (1997) toward the Scutum arm region.

3.3.4. Parameters of the Soft and Hard Components

The soft component (with the continuous absorption) makes up 76% of the total count rate in the 0.5 – 2.0 keV band. After deabsorbing the spectrum, the 0.5 – 2.0 keV band surface brightness is 2.36×10^{-8} $\text{ergs s}^{-1} \text{ cm}^{-2} \text{ sr}^{-1}$. Assuming 1 kpc of the emitting region along the line of sight, the volume emissivity is 9.6×10^{-29} $\text{ergs s}^{-1} \text{ cm}^{-3}$. The total luminosity is 1.8×10^{36} ergs s^{-1} assuming a disk-like emission region with thickness of 200 pc and a radius of 1 kpc. The modeled plasma parameters with the single absorption for the soft component are almost identical to those with the continuous absorption and thus are not separately presented in this paper.

The best fit parameters for the hard continuum are $kT = 3.67$ keV, with $N_H = 2.1 \times 10^{22}$ cm^{-2} . The hard component is responsible for 70% of the total count rate in the 2 – 10 keV band. After removing the absorption, the estimated surface brightness is 1.1×10^{-7} $\text{ergs s}^{-1} \text{ cm}^{-2} \text{ sr}^{-1}$ in the 2 – 10 keV band. Assuming ~ 15 kpc for the depth of the emitting region along the line of sight, the volume emissivity can be estimated to be $\sim 2.99 \times 10^{-29}$ $\text{ergs s}^{-1} \text{ cm}^{-3}$. For the emission volume of $\sim 1.8 \times 10^{66}$ cm^3 (assuming a thin disk with a radius of 10 kpc and a thickness of 200 pc), the 2 – 10 keV total luminosity is estimated to be $\sim 5.4 \times 10^{37}$ ergs s^{-1} .

4. DISCUSSION

The RS model appears not successful in describing the data and we found that a two component bremsstrahlung model with separate Gaussians for the candidate emission lines are more successful to describe our data. Although the inclusion of simple Gaussians in the model is rather arbitrary and

may not adequately represent the complicated spectral structure, the overall spectrum is the most effectively described with the separate Gaussian components. The fitting with separate Gaussians thus likely help represent the observed spectrum at least as an approximation. In the following sections the results are, therefore, discussed based on the model with separate Gaussians and two component bremsstrahlung.

4.1. The Soft Component

The best fit plasma temperature for the soft component is $kT = 0.92$ keV (continuous absorption) – 1.02 keV (single absorption), which is higher than that of the GXB ($kT = 0.35$ keV) (Snowden et al. 1997). Park (1998) has suggested that the foreground DXB emission (originating at $\lesssim 3$ kpc) of the $0.5 - 2$ keV band X-ray shadows in the $l, b = 10^\circ, 0^\circ$ and $l, b = 25^\circ, 0.5^\circ$ directions may arise from a $kT \sim 0.9$ keV plasma. Kaneda et al. (1997) demonstrated that the soft component of the GRXE toward the Scutum arm region ($l = 28^\circ - 29^\circ$) has a temperature of $kT = 0.8$ keV. The present results are in good agreement with these previous works. Due to the opacity of the absorbing molecular cloud, the bulk of the soft component can be assumed to arise in the foreground of the cloud. The modeled absorbing column is small ($< 5 \times 10^{21}$ cm $^{-2}$) and is in good agreement with this assumption.

Although the model fitting with the *ASCA* data is not sensitive to the low columns ($< 5 \times 10^{21}$ cm $^{-2}$) providing only an upper limit, we may further constrain the column density by using *ROSAT* results. Figure 6 compares the modeled 1.5 to 0.75 keV hardness ratios with the *ROSAT* data. Since the absorbing column is not constrained, the modeled hardness ratios are presented in a range within the upper limit ($< 5 \times 10^{21}$ cm $^{-2}$ for both continuous and single absorptions). The measured hardness ratio of the *ROSAT* data for the same region is ~ 1.4 (P98). The uncertainty of the *ROSAT* measurement (Note: this measurement is independent of the plotted N_H range in Figure 6) is displayed as the area between the dotted horizontal lines in Figure 6. The *ROSAT* measurement of the hardness ratio can be obtained in the model with $N_H \sim 3 \times 10^{21}$ cm $^{-2}$ for the continuous absorption and $N_H \sim 1 \times 10^{21}$ cm $^{-2}$ for the single absorption. Assuming a space density of 1 cm $^{-3}$, these absorbing columns imply a distance of $\lesssim 1$ kpc through the soft X-ray emitting regions. The direct comparison between the modeled flux and the measured *ROSAT* flux is complicated since the *ROSAT* data have been obtained from a mosaic of several pointings reflecting a mixture of different vignettings and responses. In Figure 6, the overall spectra with the single absorption are harder and show a larger divergence from the *ROSAT* measurement than the continuous absorption model. The harder spectra for the single absorption is perhaps as expected since the soft photons are to be more absorbed by the “single foreground” absorbing column where the same “total” absorption is considered as is with the continuous absorption. In order to demonstrate the effects of the continuous absorption, comparisons between the spectral models fitted to our data with the continuous and the single absorption (for the soft component) are presented in Figure 7 and Figure 8. Figure 7a and Figure 7b compare two models where the

“total” absorption is fixed at $1 \times 10^{21} \text{ cm}^{-2}$ for the soft component while Figure 8a and Figure 8b are where the column is $3 \times 10^{21} \text{ cm}^{-2}$. All other parameters are the best fit values to fit the data used in this paper. It is evident that the effect of the distribution of the absorbing material is small with a low column and that is more significant with a larger column where more soft photons (<1 keV) are absorbed with the single absorption. Since the single absorption with $1 \times 10^{21} \text{ cm}^{-2}$ and the continuous absorption with $3 \times 10^{21} \text{ cm}^{-2}$ have almost identical spectral shape at even below 1 keV, further distinctions between them may be infeasible even by using the *ROSAT* results. The reality is most likely in between these two extreme cases and so these two columns ($\sim 1 \times 10^{21} \text{ cm}^{-2}$ and $\sim 3 \times 10^{21} \text{ cm}^{-2}$) may represent a range of the actual absorption through the soft X-ray emitting regions.

After deabsorbing the spectrum, the average values of the modeled 0.5 – 10 keV band surface brightness, volume emissivity, and the total luminosity with the N_H in the range of $1 - 3 \times 10^{21} \text{ cm}^{-2}$ are $0.27 \times 10^{-7} \text{ ergs s}^{-1} \text{ cm}^{-2} \text{ sr}^{-1}$, $1.11 \times 10^{-28} \text{ ergs s}^{-1} \text{ cm}^{-3}$, and $0.2 \times 10^{37} \text{ ergs s}^{-1}$, respectively. The modeled average surface brightness in the 0.5 – 10 keV band ($\sim 0.27 \times 10^{-7} \text{ ergs s}^{-1} \text{ cm}^{-2} \text{ sr}^{-1}$) of the unabsorbed soft component is substantially lower than the previous result at $b = 0^\circ$ toward the Scutum arm ($\sim 2 \times 10^{-6} \text{ ergs s}^{-1} \text{ cm}^{-2} \text{ sr}^{-1}$) (Kaneda et al. 1997). It may be due to the “high” latitude of the current data (centered on $b = \sim 0.8^\circ$) as the DXB near the plane has significant flux variations along the latitudes (Kaneda et al. 1997). The low surface brightness may also indicate a soft X-ray flux variation along the Galactic longitudes. With the estimated volume emissivity the mean electron density of the plasma can be calculated by the relation, $\epsilon = n_e^2 \Lambda(T)$, where ϵ is the emissivity, and n_e is the electron density. The cooling function $\Lambda(T)$ is estimated to be,

$$\Lambda(T) = 6.2 \times 10^{-19} T^{-0.6}, \quad 0.009 \text{ keV} < kT < 3.4 \text{ keV}$$

$$\Lambda(T) = 2.5 \times 10^{-27} T^{0.5}, \quad kT > 3.4 \text{ keV}$$

(McKee & Cowie 1977). The estimated electron density is 0.0017 cm^{-3} . The thermal pressure (p/k) can then be estimated as $p/k = 2n_e T$ assuming the adiabatic phase of the plasma. In Table 2, the modeled parameters with the N_H in the range of 1 (the single absorption) – 3 (the continuous absorption) $\times 10^{21} \text{ cm}^{-2}$ are presented as an average value of each parameter for the given range of the N_H column.

4.2. The Hard Component

A hard component with $kT = 5 - 10 \text{ keV}$ ($\sim 8 \text{ keV}$ on average) has been reported for the GRXE (Koyama et al. 1986a; Kaneda et al. 1997; Yamauchi et al. 1997). The present result implies that the hard component of the Galactic X-ray background in the plane is from a $kT = \sim 3.7 \text{ keV}$ plasma. While the uncertainty associated with this temperature is large, it is still relatively lower than the previous results. The difference in the hard component temperature may be due to the assumptions in the model fittings. We have assumed an ionization equilibrium for the thermal plasma and no

contribution from a power law hard tail in the model. A broad range of the plasma temperature for the hard component has been obtained with various data depending on different assumptions within the model fittings (see §3.3.1). With the current *ASCA* data it is however infeasible to test different models and assumptions with meaningful statistics leaving such investigations in the future works.

The origin of the “lower” temperature might also be associated with the complicated Galactic structure in the $l \sim 25^\circ$ direction. The $l \sim 25^\circ$ direction of the plane has been suggested to be a “transition” region between the GXB and the molecular ring (P98). The angular extension of the molecular ring ($-60^\circ < l < 60^\circ$) (Dame et al. 1987) is coincident with that of the GRXE. The molecular ring may trace the active star-forming regions in the Galaxy and be spatially correlated with the emitting regions of the GRXE as suggested by Yamauchi & Koyama (1993). The estimated temperature of the GXB plasma is most likely $kT = 0.35$ keV (Snowden et al. 1997; Park 1998). Assuming that the $l \sim 25^\circ$ direction beyond the absorbing cloud is a transition region between the GXB and the hard component GRXE, the relatively lower temperature of the present data may reflect the existence of the “cooler” GXB plasma along the line of sight. Observations at various longitudes along the plane will be necessary to test this speculation.

Assuming that the hard component occupies a thin disk along the plane (with a thickness of ~ 200 pc, and a radius of ~ 10 kpc), the 0.5 – 10 keV total luminosity is $\sim 1.0 \times 10^{38}$ ergs s^{-1} . This total luminosity is in good agreement with the previous results for the hard component GRXE ($\sim 1 - 2 \times 10^{38}$ ergs s^{-1}) (Worrall et al. 1982; Koyama et al. 1986a; Kaneda et al. 1997; Valinia & Marshall 1998). The estimated electron density is ~ 0.0018 cm^{-3} and the thermal pressure is $p/k = 1.5 \times 10^5$ K cm^{-3} .

5. SUMMARY AND CONCLUSIONS

The Galactic X-ray background emission in the direction of $l, b = 25.6^\circ, 0.78^\circ$ is observed with *ASCA*. The observed pointing direction is toward a dense molecular cloud which casts an X-ray shadow in the 0.5 – 2 keV band. The kinematic distance to the cloud (3 kpc) and the presence of the soft X-ray shadow makes it feasible to study the spectral properties of the Galactic X-ray background emission originating in the foreground of the Galactic X-ray bulge yet beyond the Local Hot Bubble.

The observed spectrum can be fitted with a two component thermal plasma model while candidate atomic emission lines are separately fitted with narrow Gaussian profiles. The soft component is from a $kT = \sim 1$ keV plasma with low absorption and dominates the observed spectrum at < 2 keV. When compared with the *ROSAT* data, the absorbing column for the soft component is most likely in the range of $\sim 1 - 3 \times 10^{21}$ cm^{-2} depending on the specific distributions of the absorbing material along the line of sight. This range of the absorbing column implies a distance scale of $\lesssim 1$ kpc through the soft component X-ray emitting regions. These results indicate that the

0.5 – 2 keV soft X-ray background emission in the Galactic plane arises from an $\sim 10^7$ K thermal plasma within ~ 1 kpc from the Sun, at least in the $l \sim 25^\circ$ direction.

The hard component is from a $kT = \sim 3.7$ keV plasma and absorbed by the Galactic disk. The best fit temperature is relatively lower compared to the previous studies of the GRXE. The difference in the continuum temperature may reflect the assumptions in the given model fitting or may be due to the complexity of the Galactic DXB emitting regions along the line of sight. Follow up observations of the Galactic DXB for various directions along the plane with *XMM-Newton* and/or *Chandra* will be necessary to address the complicated nature of the Galactic DXB along the plane.

The authors thank S. Snowden for valuable discussion, and A. Valinia for helpful comments at the early stage of this work. We also thank the referee for the constructive comments. This work was supported by USRA and NASA Cooperative Agreement NCC 5-356.

REFERENCES

- Almy, R. C., McCammon, D., Digel, S. W., Bronfman, L., & May, J. 2000, ApJ, in press
- Cox, D. P. & Reynolds, R. J. 1987, ARA&A, 25, 303
- Chen, L.-W, Fabian, A.C., & Gendreau, K. C. 1997, MNRAS, 285, 449
- Dame, T. M., Ungerechts, H., Cohen, R.S., de Geus, E. J., Grenier, I. A., May, J., Murphy, D. C., Nyman, L. -Å, & Thaddeus, P. 1987, ApJ, 322, 706
- Gendreau, K. C. 1995, Ph.D. Thesis, Massachusetts Institute of Technology
- Ishisaki, Y. 1996, Ph.D. Thesis, University of Tokyo
- Jakobsen, P. & Kahn, S. M. 1986, ApJ, 309, 682
- Kaneda, H. 1996, Ph.D. Thesis, University of Tokyo
- Kaneda, H., Makishima, K., Yamauchi, S. Koyama, K., Matsuzaki, K., & Yamasaki, N. Y. 1997, ApJ, 491, 638
- Koyama, K., Makishima, K., Tanaka, Y., & Tsunemi, H. 1986a, PASJ, 38, 121
- Koyama, K., Ikeuchi, S., & Tomisaka, K. 1986b, PASJ, 38, 503
- McKee, C. F., & Cowie, L. L. 1977, ApJ, 215, 213
- Morrison, R. & McCammon, D. 1983, ApJ, 270, 119
- Nousek, J. A., Fried, P. M., Sanders, W. T., & Kraushaar, W. L. 1982, ApJ, 258, 83

- Ottmann, R., & Schmitt, J. H. M. M. 1992, *A&A*, 256, 421
- Park, S., Finley, J. P., Snowden, S. L., & Dame, T. M. 1997, *ApJ*, 476L, L77
- Park, S. 1998, Ph.D. Thesis, Purdue University
- Park, S., Finley, J. P., & Dame, T. M. 1998, *ApJ*, 509, 203 (P98)
- Schmitt, J. H. M. M. & Snowden, S. L. 1990, *ApJ*, 361, 207
- Serlemitsos, P. J., Jalota, L., Soong, Y., Kunieda, H., Tawara, Y., Tsusaka, Y., Suzuki, H., Sakima, Y., Yamazaki, T., Yoshioka, H., Furuzawa, A., Yamashita, K., Awaki, H., Itoh, M., Ogasaka, Y., Honda, H., & Uchibori, Y. 1995, *PASJ*, 47, 105
- Smith, R., 1999, private communications
- Snowden, S. L., McCammon, D., Burrows, D. N., & Mendenhall, J. A. 1994, *ApJ*, 424, 714
- Snowden, S. L., Egger, R., Freyberg, M. J., McCammon, D., Plucinsky, P. P., Sanders, W. T., Schmitt, J. H. M. M., Trümper, J., & Voges, W., 1997, *ApJ*, 485, 125
- Snowden, S. L., Egger, R., Finkbeiner, D. P., Freyberg, M. J., & Plucinsky, P. P. 1998, *ApJ*, 493, 715
- Valinia, A., & Marshall, F. E. 1998, *ApJ*, 505, 134
- Valinia, A., Tatischeff, V., Arnaud, K., Ebisawa, K., & Ramaty, R. 2000, *ApJ*, in press
- Wang, Q. D. 1992, *ApJ*, 392, 509
- Warwick, R. S., Turner, M. J. L., Watson, M. G., & Willingale, R. 1985, *Nature*, 317, 218
- Worrall, D. M., Marshall, F. E., Boldt, E. A., & Swank, J. H. 1982, *ApJ*, 255, 111
- Yamasaki, N. Y., Ohashi, T., Takahara, F., Yamauchi, S., Koyama, K., Kamae, T., Kaneda, H., Makishima, K., Sekimoto, Y., Hirayama, M., Takahashi, T., Yamagami, T., Gunji, S., Tamura, T., Miyazaki, S., & Nomachi, M. 1997, *ApJ*, 481, 821
- Yamauchi, S., & Koyama, K. 1993, *ApJ*, 404, 620
- Yamauchi, S., & Koyama, K. 1995, *PASJ*, 47, 439
- Yamauchi, S., Kaneda, H., Koyama, K., Makishima, K., Matsuzaki, K., Sonobe, T., Tanaka, Y., & Yamasaki, N. Y. 1997, *X-ray Imaging and Spectroscopy of Cosmic Hot Plasmas* Proceedings of International Symposium on X-ray Astronomy, edited by F. Makino & K. Mitsuda, (Universal Academy Press, Inc. Tokyo, Japan), 145

Table 1. Best fit parameters for bremsstrahlung + Gaussian model.

	Continuous	absorption	Single	absorption
	N_H	kT	N_H	kT
	(10^{22} cm $^{-2}$)	(keV)	(10^{22} cm $^{-2}$)	(keV)
Soft	<0.48 ^a	$0.92^{+0.41}_{-0.39}$	<0.51 ^a	$1.02^{+0.47}_{-0.46}$
Hard	2.1 ^b	3.67 ^b	2.1 ^b	3.67 ^b
$\chi^2_\nu=0.45$			$\chi^2_\nu=0.45$	

^aThis is a 2σ upper limit.

^bThis is the best fit value from the hard component fit in the 3 – 9 keV band and is fixed in the overall fitting.

Table 2. Summary of modeled plasma parameters for the soft and hard components after removing the absorption.

Parameter	Soft ^{a,b}	Hard ^a
Surface Brightness (ergs s ⁻¹ cm ⁻² sr ⁻¹)	0.27×10^{-7}	1.89×10^{-7}
Volume Emissivity (ergs s ⁻¹ cm ⁻³)	1.11×10^{-28}	0.51×10^{-28}
Total Luminosity (ergs s ⁻¹)	0.2×10^{37}	0.94×10^{38}
Electron Density (cm ⁻³)	0.0017	0.0018
Thermal Pressure (p/k , K cm ⁻³)	3.6×10^4	1.5×10^5

^aThese are derived from the 0.5 – 10.0 keV band.

^bThese are the average values for each model parameter where N_H is in the range of $1 - 3 \times 10^{21}$ cm⁻².

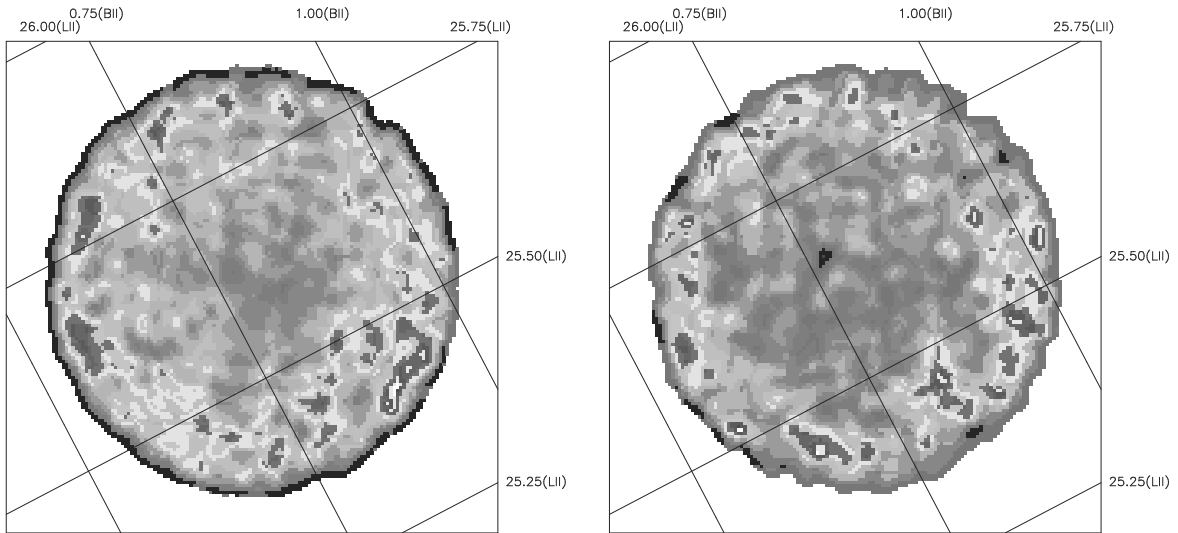


Fig. 1.— *Left:* (a) The exposure and vignetting corrected 2.0 – 9.0 keV band *ASCA* (GIS2+GIS3) image. *Right:* (b) The exposure and vignetting corrected 0.8 – 2.0 keV band *ASCA* (GIS2+GIS3) image. Both images are smoothed with a Gaussian with $\sigma=2$ pixels.

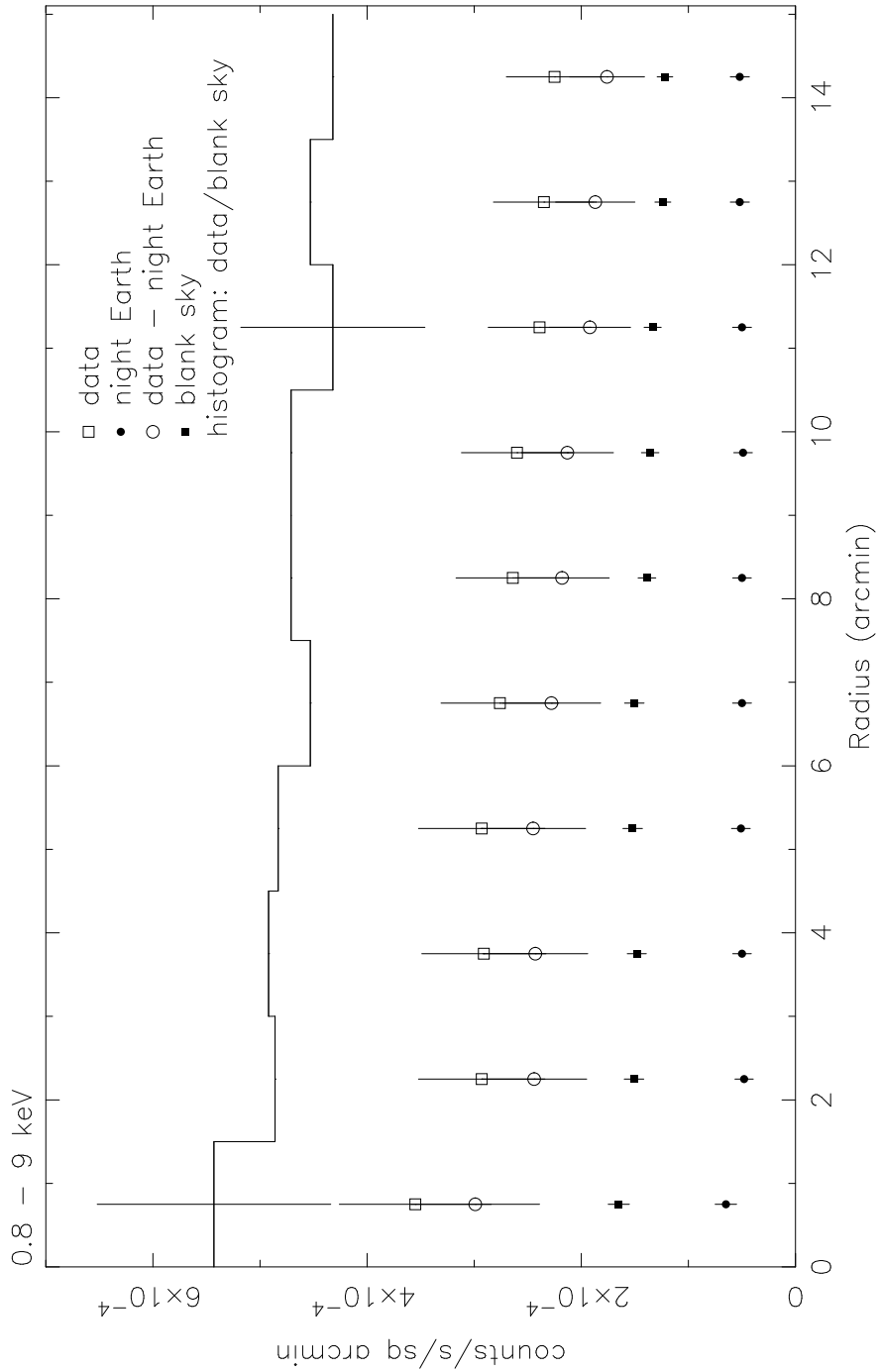


Fig. 2.— Radial profiles of the 0.8 - 9 keV DXB from the GIS. The count rates are integrated over the annular bins of $1.5'$ within the $15'$ radius region. The night-Earth subtracted data to blank-sky ratio as presented with histograms has been arbitrarily scaled to fit the display window. The vertical lines on the histogram present typical errors.

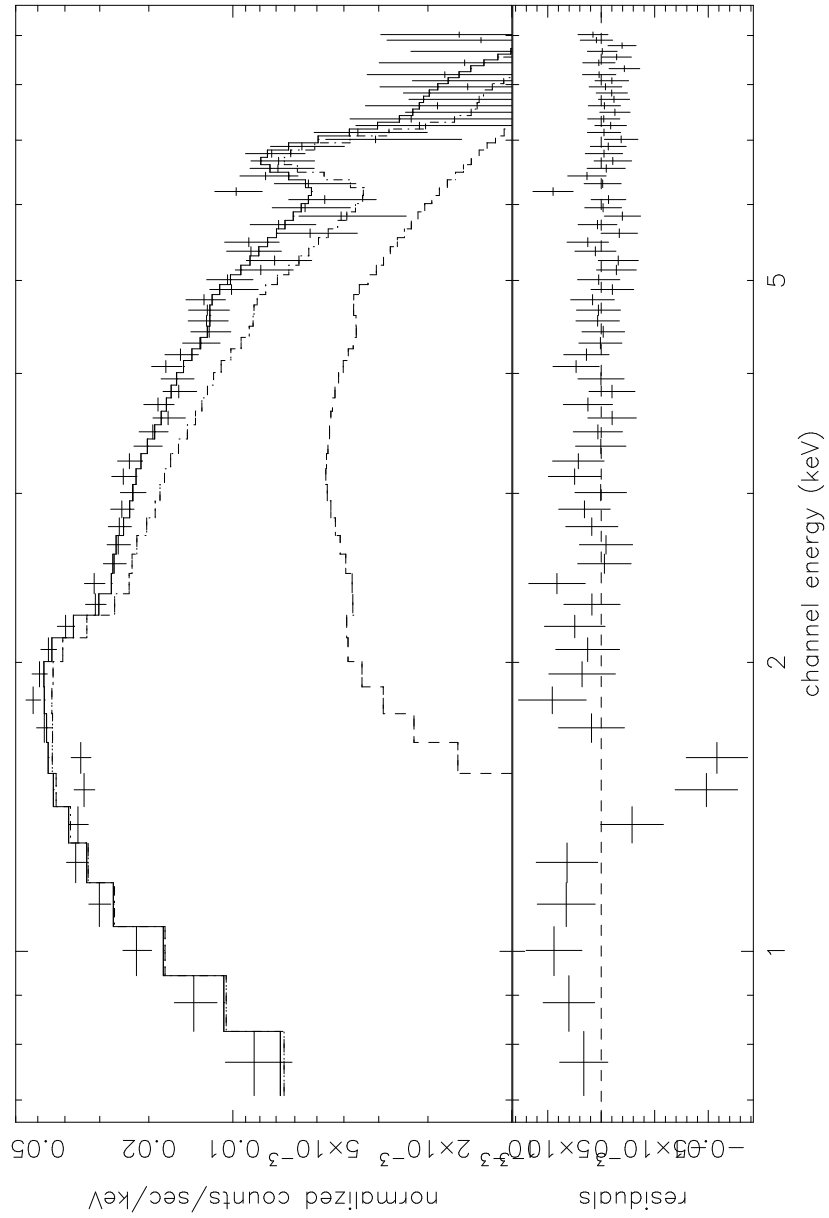


Fig. 3.— The ASCA/GIS spectrum folded through the instrumental response with the best-fit one component Raymond-Smith model. The dashed line represents the fixed extragalactic power law component.

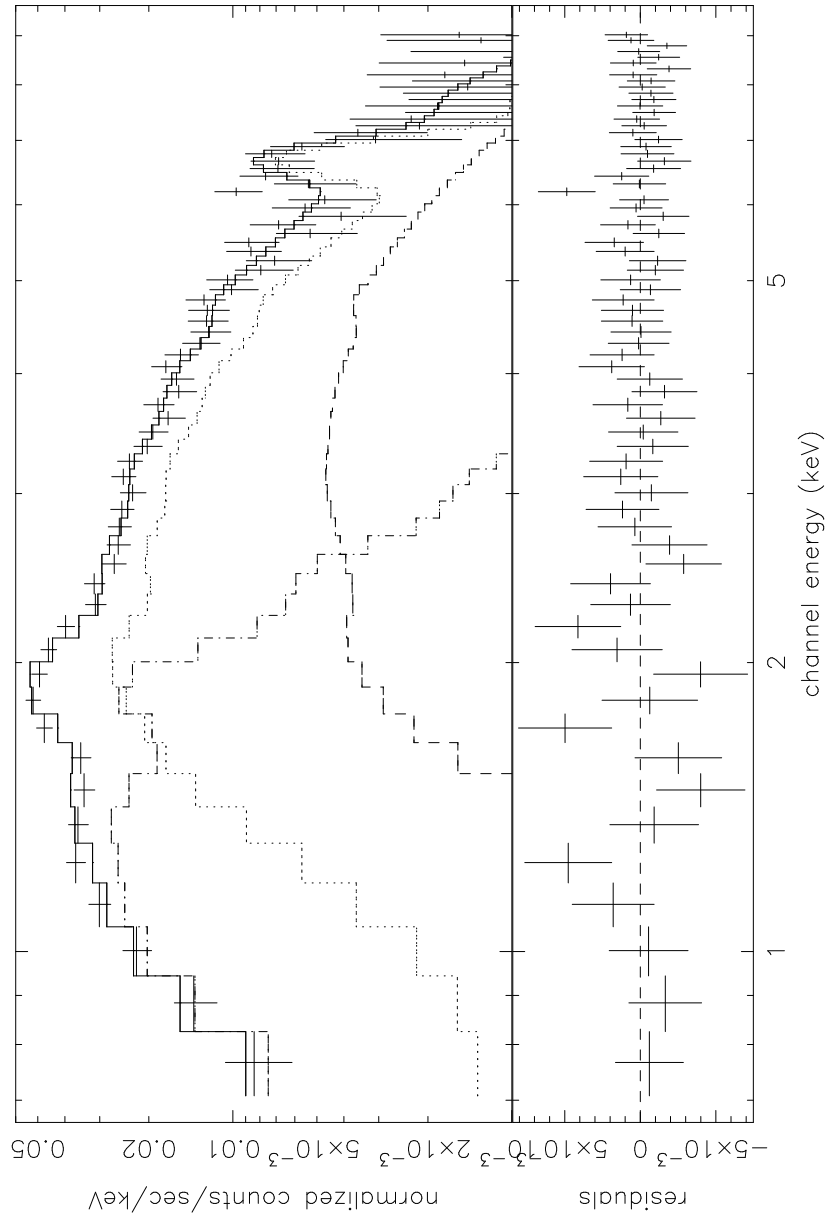


Fig. 4.— The ASCA/GIS spectrum folded through the instrumental response with the best-fit two component Raymond-Smith model. The dashed line is the fixed extragalactic power law. The dot-dashed line represents the best fit soft component of the Raymond-Smith and the dotted line is the best fit hard component of the Raymond-Smith model.

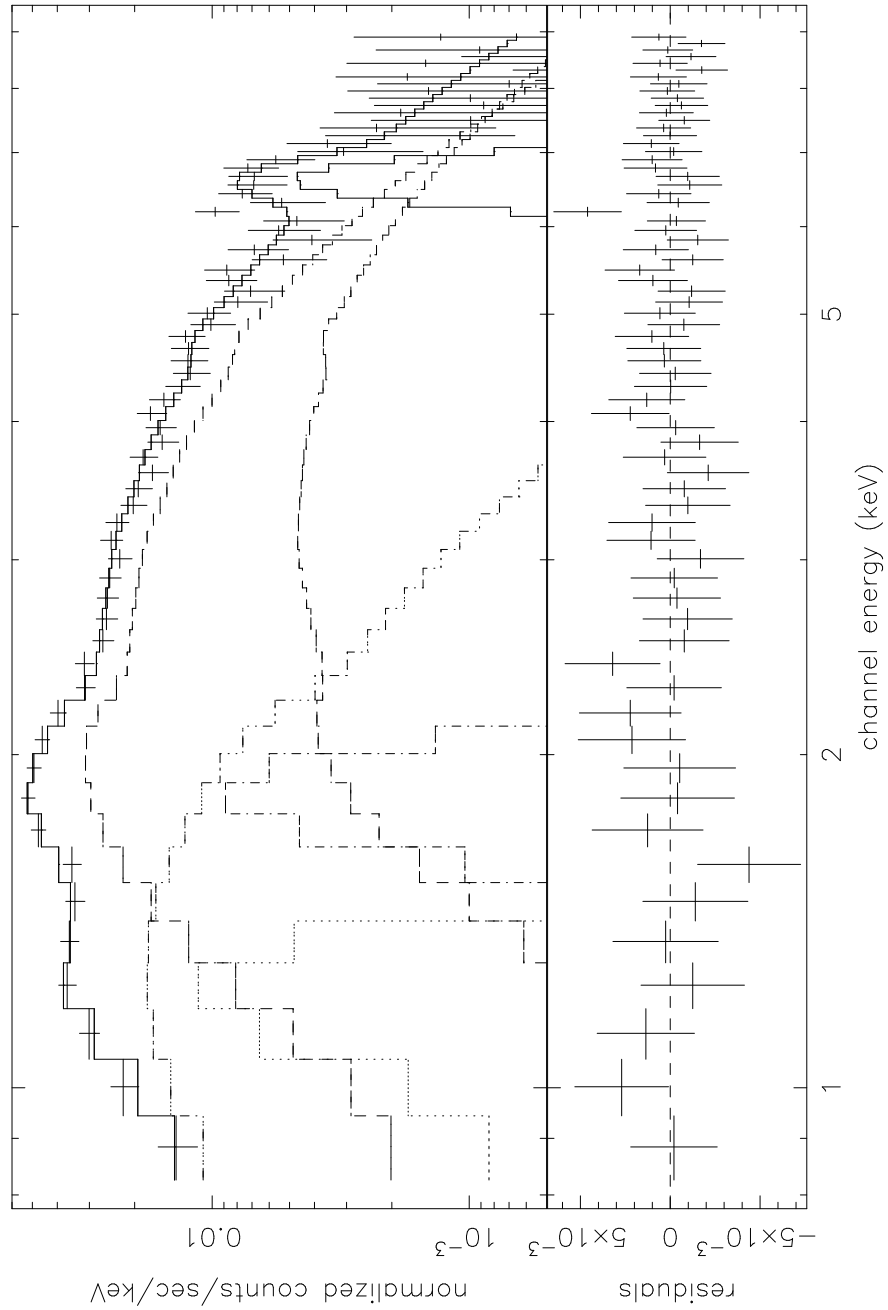


Fig. 5.— The ASCA/GIS spectrum folded through the instrumental response with the best-fit two component thermal bremsstrahlung (with the continuous absorption for the soft component). Candidate atomic emission lines are fitted with separate Gaussians.

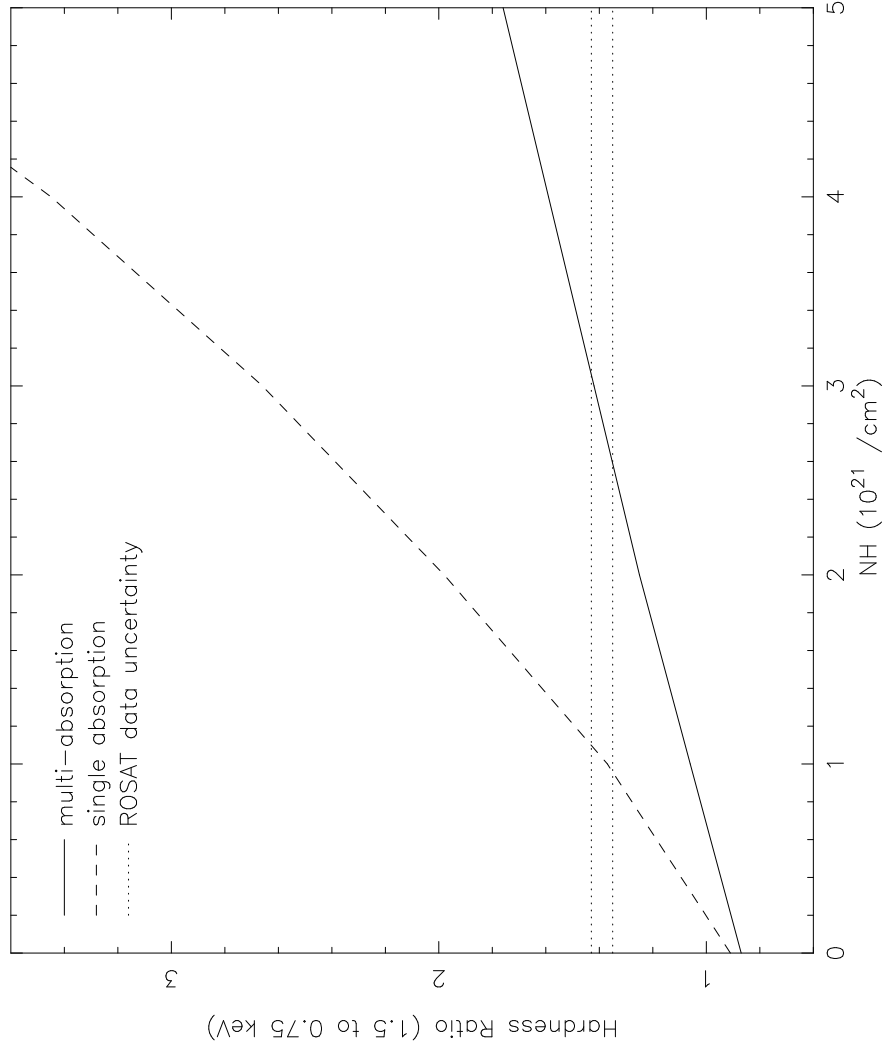


Fig. 6.— The modeled 1.5 to 0.75 keV hardness ratios. The solid line is for the continuous absorption model, and the dashed line is for the single absorption model. The area between the horizontal dotted lines presents the *ROSAT* measurement for the same region with embedded uncertainty.

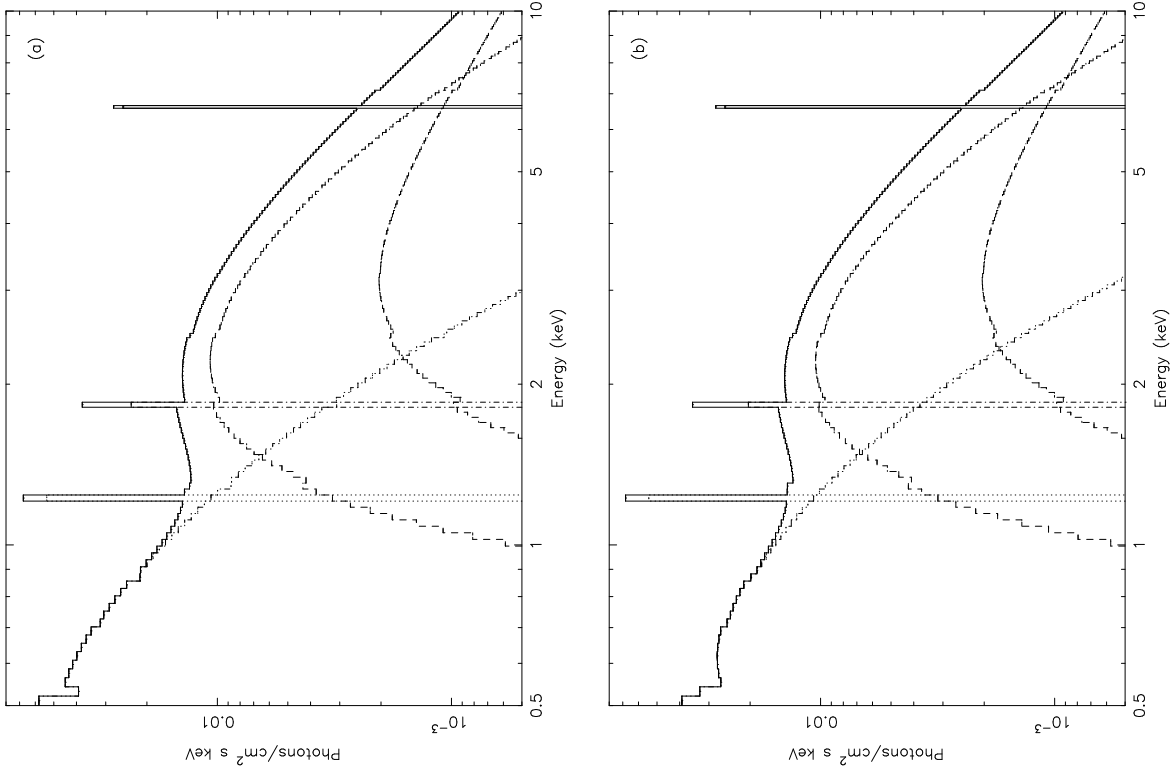


Fig. 7.— The fitted model spectra with absorbing column fixed at $1 \times 10^{21} \text{ cm}^{-2}$ for the soft component. All other parameters are fixed at the best fit values as presented in Section §3.3.3. Panel (a) is with a continuous absorption and (b) is with a single absorption for the soft component.

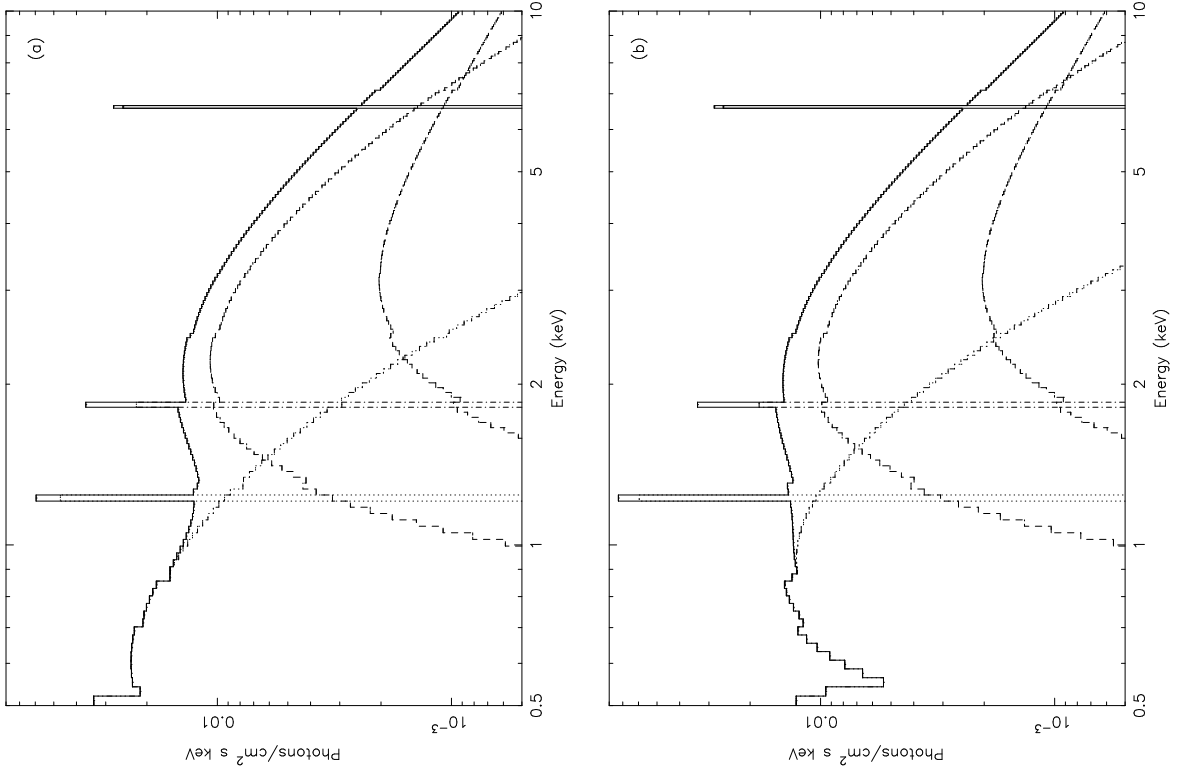


Fig. 8.— The fitted model spectra with absorbing column fixed at $3 \times 10^{21} \text{ cm}^{-2}$ for the soft component. All other parameters are fixed at the best fit values as presented in Section §3.3.3. Panel (a) is with a continuous absorption and (b) is with a single absorption for the soft component.